

## Dependence of the electrochemical parameters of composite SiO/C anodes for lithium-ion batteries on the composition and synthesis temperature

© D.A. Lozhkina, E.V. Astrova, A.M. Rumyantsev

Ioffe Institute,  
194021 St. Petersburg, Russia  
e-mail: darina.lozhka94@gmail.com

Received September 24, 2021

Revised November 23, 2021

Accepted November 24, 2021

The results of a study of anodes obtained by carbonization of silicon monoxide by means of a reaction with solid-phase fluorocarbon  $\text{CF}_{0.8}$  are presented. Charge/discharge voltage profiles were studied at different currents depending on the composition and temperature of the synthesis of composites. The irreversible losses of the 1st cycle and the contribution to them of intrinsic losses due to the formation of lithium oxide and its silicates and losses associated with the formation of SEI are analyzed. A difference has been established in the behavior of anodes made of SiO carbonized by annealing with  $\text{CF}_{0.8}$  at  $T = 800^\circ\text{C}$  (SiO/C composite) and silicon monoxide annealed with  $\text{CF}_{0.8}$  at  $T > 1000^\circ\text{C}$  at which disproportionation occurs simultaneously with the carbonization of SiO (*d*-SiO/C composite). The difference consisting in a higher discharge capacity, a higher Coulomb efficiency, and better rate capability of *d*-SiO/C is explained by a change in the composition of the  $\text{SiO}_x$  matrix that occurs during the disproportionation process. The effect of the formation of *d*-SiO/C anodes by preliminary lithiation with a low current, after which the electrodes can be charged and discharged with much higher currents, has been discovered. The effect is explained by the amorphization of silicon crystallites and the increasing diffusion coefficient of lithium.

**Keywords:** composite anodes SiO/C, lithium-ion batteries, disproportionation silicon monoxide, carbonization with fluorocarbon.

DOI: 10.21883/TP.2022.03.53264.267-21

### Introduction

Non-stoichiometric silicon oxides  $\text{SiO}_x$  are alternative anode materials to silicon for lithium-ion batteries (LIB) [1–4]. Their usage allows to control electrochemical parameters by means of control of components, non-active relating to lithium. During the first lithiation SiO conversion reaction happens with formation of silicates and lithium oxide (irreversible phases). As a result of this conversion the nano-scale silicon appears, that reversibly reacts with lithium, forming the intermetallic compounds of  $\text{Li}_x\text{Si}$  [5–9]. Irreversible phases, first of all, act as buffer matrix of the volume, changed during lithiation and delithiation process, and restrict amount of implemented Li. For  $\text{Li}_{15}\text{Si}_4$  phase the initial volume expansion is about 400% [10], that is  $\sim 2$  bigger compared to what happens during lithiation of SiO [2,11]. Secondly, it is considered, that anodes, made of silicon monoxide, have higher charge transfer velocity than Si and even graphite [12], that is important for improving the rate capability. According to authors of [9], this is because of the formed lithium silicates, and as per data from review [2] — because of high coefficient of diffusion of  $\text{Li}^+$  in  $\text{Li}_2\text{O}$ . However, despite the existing advantages, silicon oxides have some disadvantages, preventing from their use. Formation of irreversible phases results in relatively low initial Coulomb efficiency. Silicon oxides are insulators with low electrical conductivity, that reduces the electrochemical

activity of  $\text{SiO}_x$  anodes. The problem of volume change in case of  $\text{SiO}_x$  is not so serious as for Si, but it can not be neglected. To solve such problems the various strategies were developed, such as the creation of composites, among which the special attention is made to carbon composites of  $\text{SiO}_x/\text{C}$  [2,13–18].

In this work for SiO/C anodes formation we used the recently proposed method of silicon and its oxides carbonization at their interaction with solid-phase fluorocarbon  $\text{CF}_{0.8}$  in Ar atmosphere [19–21]. Reactions with formation of gaseous products, appearing at interaction of  $\text{CF}_{0.8}$  with silicon monoxide, allow to obtain the composite porous material with carbon shell around SiO particles. Properties of such anode material can be studied in „clear form“ without additional components, used in slurry technology, since electrodes are made as tablets. Another specific of the process is a partial disproportionation of silicon monoxide to Si and  $\text{SiO}_2$  (*d*-SiO formation), that happens simultaneously with carbonization at  $T > 1000^\circ\text{C}$ , and at higher temperatures — formation of silicon carbide of cubic polytype, including in the form of whiskers of SiC [21], on the tablets surface. In the work [22] the influence of annealing temperature on electrochemical parameters of SiO/C anodes, made of mixture, containing 40% SiO and 60%  $\text{CF}_{0.8}$ , was studied. In this work the concentration and temperature dependencies of electrochemical parameters of composite anodes are reported.

## 1. Experiment

The initial material for SiO/C synthesis was the commercial products of SiO silicon monoxide of High Purity grade and carbon fluoride of CF<sub>0.8</sub> composition (Halopolymer). Powders, taken in proper weight proportion, were thoroughly mixed and grinded in agate mortar. From the resulting mixtures at pressure of 180 MPa the tablets with diameter of 10 mm were pressed and annealed in quasi-closed volume of graphite cassettes. The cassettes were put into a muffle furnace with a quartz tube, heated to 400°C and purged with high purity argon (99.998%). Then the slow temperature increase was performed with a rate of 3.3 grad/min until the specified temperature in a range of  $T = 800\text{--}1100^\circ\text{C}$ , with the following exposure for one hour and cooling in Ar on the tube edge for 30 min.

Before and after annealing the weighting, measurement of thickness and area of the resulting tablets were performed, from which the density  $\rho$  was defined. Specific surface of samples  $S_{\text{specific}}$  was defined using BET method (Brunauer, Emmett and Teller) as per nitrogen adsorption isotherm at temperature of 77 K using adsorption-structure analyzer ASAP 2020 made by Micromeritics.

To make electrodes from the resulting tablets their thickness was reduced by grinding to  $\sim 100\ \mu\text{m}$ , their area varied from 30 to 50 mm<sup>2</sup>, weight of the tested samples was 2–5 mg. After that the samples were glued to a copper foil with suspension based on polyvinylidene fluoride (PVDF), highly-split graphite and NMP (N-methylpyrrolidone) with the subsequent cutting to a cell diameter.

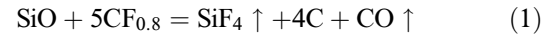
Galvanostatic measurements were performed in two-electrode disc cells CR2032 with diameter of 15 mm with lithium counter electrode by using CT3008W-5V10mA stand (Neware). Tinci TC-E918 product, that is a 1 M solution of LiPF<sub>6</sub> in a mixture of EC/PC/DEC/EMC/PA (ethylene carbonate, propylene carbonate, diethyl carbonate, ethylmethyl carbonate, propyl acetate), was used as an electrolyte. Charge (lithiation) and discharge (lithium extraction) of electrodes at the first cycle were performed usually with a current density  $j = 10\ \text{mA/g}$ . Charge was restricted with a voltage of 10 mV, discharge — with a voltage of 2 V.

Impedance measurements were performed using modular potentiostat/galvanostat, made by Biologic VSP, within the frequency range  $\nu$  from 100 kHz to 0.01 Hz, alternating voltage amplitude was 7 mV. Measurements were performed in two-electrode cells with lithium counter electrode, polarization of which can be neglected, since the samples charge was made with low current.

## 2. Composition and physical properties of SiO/C composites

Interaction of SiO and non-stoichiometric carbon monofluoride CF<sub>0.8</sub> is performed at temperature of

400–650°C [21]. In this work the relatively low temperatures of  $< 1100^\circ\text{C}$  were used for SiO carbonization, when amount of the resulting silicon carbide is low and can be neglected [22]. Then, according with the reaction



at stoichiometric composition of initial mixture of 24.5% SiO + 75.5% CF<sub>0.8</sub> only the carbon remains in the solid phase. To obtain SiO/C composite, the reaction product should contain silicon monoxide, that should be taken in excess. For arbitrary relation of initial components, where  $r$  is fluorocarbon content in weight percentage, the equation (1) can be expressed the following way:

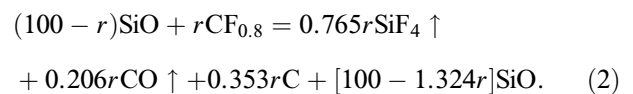


Figure 1, *a* shows the calculated dependence of SiO and C concentration in the resulting composite depending on amount of silicon monoxide in the initial mixture. Starting from temperature of 1000°C, beside the interaction with fluorocarbon, the SiO disproportionation occurs simultaneously



Amount of silicon and size of its precipitates, formed within the same one-hour annealing of SiO at various temperature, was defined by using a quantitative XRD analysis from the work [23].

The initial density of the pressed tablets, regardless of SiO concentration, was  $\sim 1.4\ \text{g/cm}^3$ , after annealing its value decreased due to formation of gaseous reaction products of SiF<sub>4</sub> and CO. Experimental values of relative weight loss reduced with SiO amount increase in the initial material (ini SiO), that is in good agreement with calculation data (Fig. 1, *b*). Therefore, the density of the annealed tablets  $\rho$  increased (Fig. 2, *a*), while porosity  $p$  decreased (Fig. 2, *b*), remaining almost the same for both annealing temperatures of 800 and 1050°C. The average porosity of the tablets was evaluated as per formula  $p = 1 - \rho/\rho_{\text{mix}}$ , where  $\rho_{\text{mix}}$  is calculated density of a compact mixture of a known composition: (CF<sub>0.8</sub> + SiO) before annealing and (C + SiO) after annealing. During calculation of  $\rho_{\text{mix}}$  the following values were used for their components density:  $\rho_{\text{CF}_{0.8}} = 2.94\ \text{g/cm}^3$  [24],  $\rho_{\text{SiO}} = 2.13\ \text{g/cm}^3$ ,  $\rho_{\text{C}} = 1.86\ \text{g/cm}^3$  (soot density). Figure 2 shows that heat treatment temperature increase from 800 to 1050°C has a little effect on density and porosity of the composites.

Internal surface area  $S$  was measured for samples with 40 and 70% SiO in the initial mixture, that were annealed at three different temperatures. For comparison  $S$  was also defined for the initial SiO powder after fining, that was extremely low compared to composite materials. According to data, presented in Table 1, the more carbon in the composite, the higher surface area, i.e. nanocrystalline carbon, formed on a surface of SiO particles [22], makes

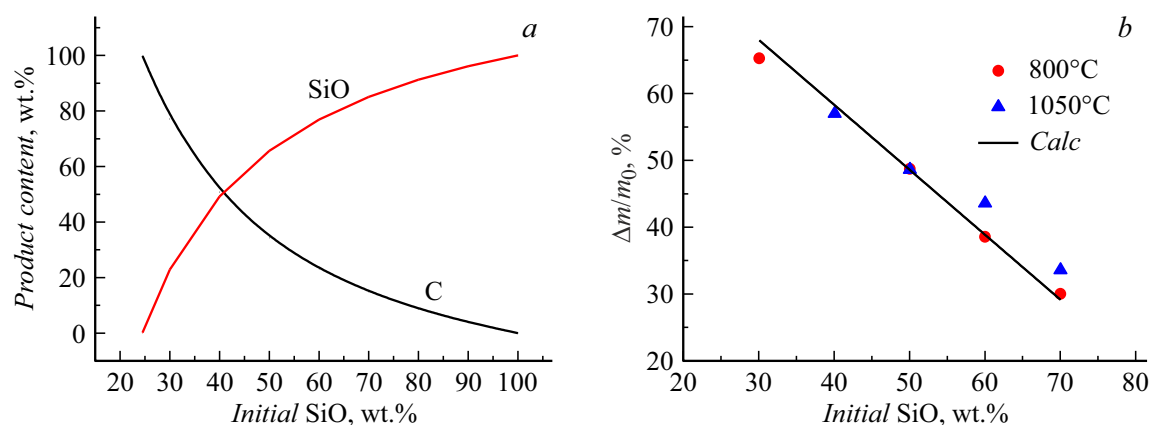


**Figure 1.** Concentration dependence on SiO percentage content in initial mixture: *a* — of reaction products (2), of silicon monoxide and carbon; *b* — of relative weight loss for samples, annealed at  $T = 800$  and  $1050^\circ\text{C}$  (experimental and calculated values).

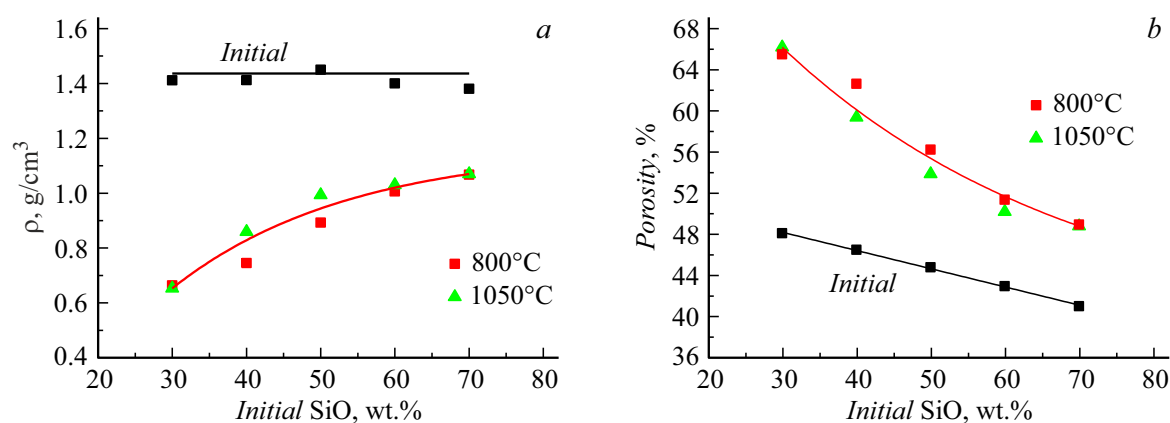


**Figure 2.** Dependence of density (*a*) and porosity (*b*) of samples on initial concentration of SiO before and after annealing at  $T = 800$  and  $1050^\circ\text{C}$ .

**Table 1.** Specific surface area of samples, annealed at various temperature

$T$ of annealing, $^\circ\text{C}$	$S$ , $\text{m}^2/\text{g}$ 40%SiO	$S$ , $\text{m}^2/\text{g}$ 70%SiO	$S$ , $\text{m}^2/\text{g}$ 100%SiO
—			0.36
800	252	62.8	
1050	222	54.9	
1100	213	53.2	

the biggest contribution to this area. Annealing temperature increase slightly reduces  $S$ , that seemingly is related to a sintering process, accompanied with closing of some quantity of pores.

Specific electrical resistance  $\rho_{el}$  of composites of various composition was evaluated based on resistance of annealed tablets before their thinning. According to Table 2, the increase of carbon content results in significant reduction of the samples specific resistance.

**Table 2.** Specific resistance of tablets, annealed at  $1050^\circ\text{C}$ , depending on initial composition of mixture and carbon content in finished SiO/C composite

SiO <sub>ini</sub> , w%	C (1050°), w%	$\rho_{el}$ , $\Omega\cdot\text{cm}$
30	77.1	82
40	50.7	110
50	34.2	178
60	23.0	2300
70	14.9	1600

### 3. Influence of SiO/C composition on electrochemical parameters of anodes

Figure 3 shows charge/discharge curves of the 1st cycle for composite anodes of various composition, annealed at temperatures, corresponding to carbonization at  $800^\circ\text{C}$  (SiO/C formation) and carbonization combining with disproportionation at  $1050^\circ\text{C}$  ( $d\text{-SiO/C}$  formation).

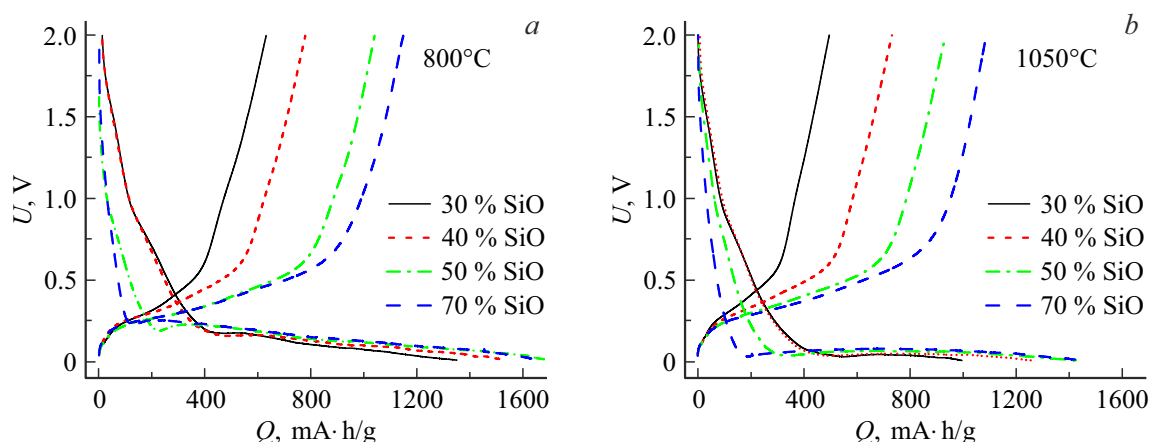
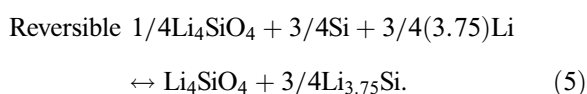
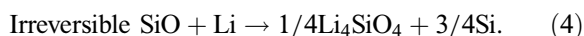


**Figure 3.** Galvanostatic charge/discharge curves of the 1st cycle for SiO/C (a) and *d*-SiO/C (b) anodes, made from initial mixtures with various SiO content. Current density is 10 mA/g.

It is obvious, that with SiO content increase in the initial mixture there is an increase of charge and discharge capacity and variation of charge curves shape: for samples with high SiO content at the initial section there is a rather sharp drop of voltage with reaching the plateau, that is specific for silicon-based electrodes. In samples with high carbon content the initial section becomes mildly sloping and at  $U \approx 0.9$  V there is a curve slope change on it, as in carbon materials [25]. Comparing charge/discharge curves for SiO/C and *d*-SiO/C samples, it can be noted, that in the first case both charge and discharge curves are located a bit higher in terms of voltage, than in the second case, and transition to long flat section on the charge curve starts at higher potential, furthermore this section has the higher slope.

Figure 4 shows the dependence of charge and discharge capacities of the first cycles for SiO/C anodes depending on initial SiO content. For comparing with experimental values of charge capacity the dependence is shown, calculated as per formula  $Q_{\text{ch}}(\text{calc}) = 2680s + 375(1 - s)$ , where  $Q = 2680$  mA·h/g is theoretical capacity of SiO in assumption, that Li reacts with all silicon in it, 375 mA·h/g is carbon capacity,  $s$  is portion of SiO in the finished composite. Experimental discharge capacity is compared with reversible capacity of composite, calculated as  $Q_{\text{dch}}(\text{calc}) = 1700s + 375(1 - s)$ , where 1700 mA·h/g is reversible capacity of SiO, obtained from reactions, happened during the first lithiation [1]:



In both cases during calculation it was assumed, that lithium with silicon forms alloy of  $\text{Li}_{3.75}\text{Si}$  composition. Calculated and experimental dependencies display the sim-

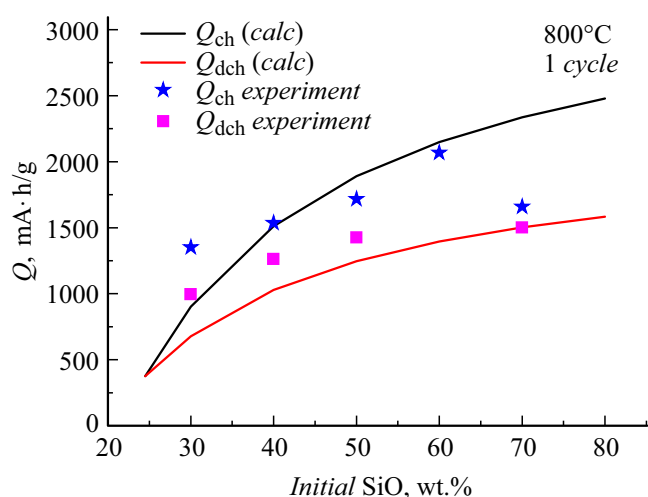


**Figure 4.** Charge and discharge capacity of the 1st cycle depending on SiO content in initial mixture: dots are experimental values, lines are calculated values.

ilar trend of capacity increase with increase of percentage content of silicon monoxide in the initial mixture.

Coulomb efficiency (CE) of the 1st cycle increases with increase of ini SiO content (Fig. 5), while for 1050-degr. samples in the whole concentration range CE is somewhat higher. This is caused by reduction of irreversible losses due to transformation at disproportionation the part of SiO into non-active  $\text{SiO}_2$  [26,27]. Low CE in samples with high carbon content (small SiO content) is caused by high SEI losses, related to carbon with large surface area (Table 1).

For samples of SiO/C and *d*-SiO/C with various initial concentration of silicon monoxide the measurements of their rate capability were performed. For that, at first, for 5 cycles the electrodes were cycled at current density  $j = 10$  mA/g, after which the charge and (or) discharge current density was increased (numerator and denominator in decimals in Fig. 6 respectively). Figure 6 shows that

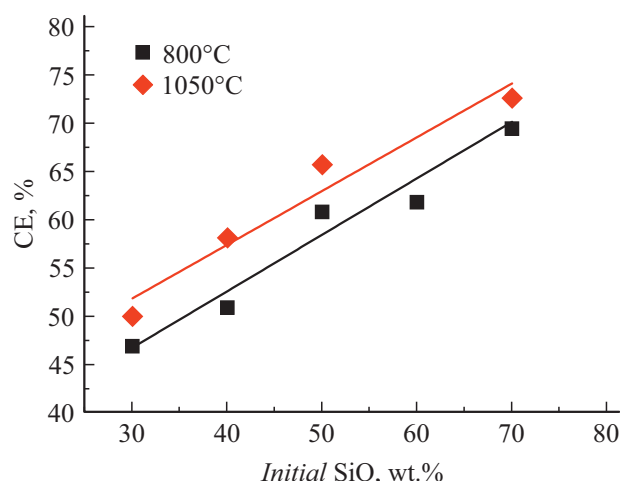


**Figure 5.** Coulomb efficiency of the 1st cycle for SiO/C and *d*-SiO/C anodes depending on initial composition.

with current increase there is a sharp drop of capacity for samples with high SiO content. Return at 18th cycle to mode with  $j = 10$  mA/g results in capacity increase, while for samples with 30, 40 and 50% SiO the discharge capacity returns to almost initial value. *d*-SiO/C composites are more stable, while the absolute value of capacity is lower for them. It seems, it is related to damping action of silicon dioxide non-active to Li [27]. Samples with initial content of 30–50% SiO behave better in both cases — for SiO/C and *d*-SiO/C.

#### 4. Dependence on composites formation temperature

Figure 7 shows charge/discharge curves of the 1st cycle for samples of two compositions, annealed at various temperature. It can be observed, that disproportionation

of silicon monoxide results in decrease of charge and discharge capacities for *d*-SiO/C (1050°) compared to SiO/C (800°) electrodes and almost complete impossibility to insert lithium into samples, annealed at  $T \geq 1100^\circ\text{C}$ .

With annealing temperature increase the flat section of charge curves shifts towards lower voltage  $U$ , resulting in decrease of voltage  $U_b$ , that we considered as the start of this section. As a result, at first lithiation the voltage at high-temperature samples ( $T \geq 1100^\circ\text{C}$ ) reaches the specified limit of 10 mV earlier, than reaches the plateau, when electrode gets the larger part of capacity, and it is impossible to charge it proper way (see blue curves 1100 in Fig. 7 (in online version)). Similar behavior of electrodes of *d*-SiO after disproportionation at  $T \geq 1100^\circ\text{C}$  was observed by the authors of [28]. In our experiments the decrease of current density in half to 5 mA/g resulted in successful charge of all high-temperature samples. Figure 8 shows charge and discharge curves for 1100-degr. samples, recorded for the 1st cycle at current mode of 10 mA/g, 2nd at 5 mA/g (forming), and 3rd cycle again at 10 mA/g. Thus, high-temperature samples of *d*-SiO/C after preliminary forming with low value of  $j$  are capable to operate further at higher current densities.

It should be noted, that the shape of the charge curve with sloped flat section, specific for cycle 3, also remains at the following cycles. In *d*-SiO/C electrodes, annealed at  $T < 1100^\circ\text{C}$  and not required preliminary forming, this slope appeared at the 2nd cycle already (Fig. 9) and remained at the following cycles. Coulomb efficiency after the first cycle gradually increases and at the 5th cycle reaches 93 and 95.3% respectively for SiO/C and *d*-SiO/C composites.

Let's analyze the charge/discharge curves of Fig. 7. Figure 10 shows dependence of voltage  $U_b$  on annealing temperature. Its shifting is compared with variation of  $\text{SiO}_x$  matrix composition, that happens due to Si precipitation [23]. According to the plots  $U_b = f(T)$  and  $x = f(T)$ , with increase of annealing temperature  $U_b$  shifts to lower

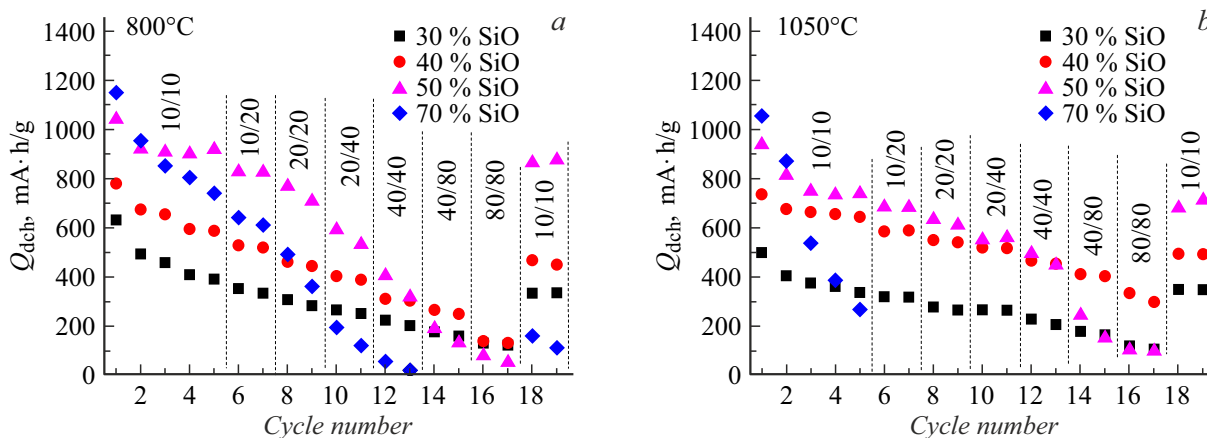


**Figure 6.** Discharge capacity of SiO/C (a) and *d*-SiO/C anodes (b) depending on cycle number at various current of charge (specified in numerator) and discharge (in denominator)  $j$ , [mA/g].

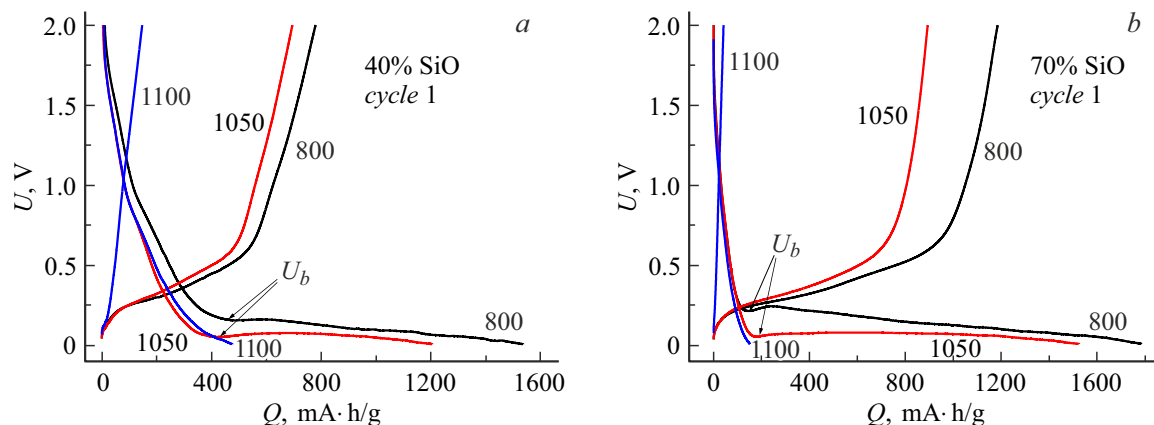


**Figure 7.** Charge/discharge curves of the 1st cycle for electrodes, annealed at various temperature: *a* — with initial composition of 40% SiO and *b* — 70% SiO,  $j = 10$  mA/g. For the purpose of illustration simplification only the curves for three annealing temperatures are shown: 800, 1050 and 1100°C.  $U_b$  is voltage of charge curve transition to flat section.

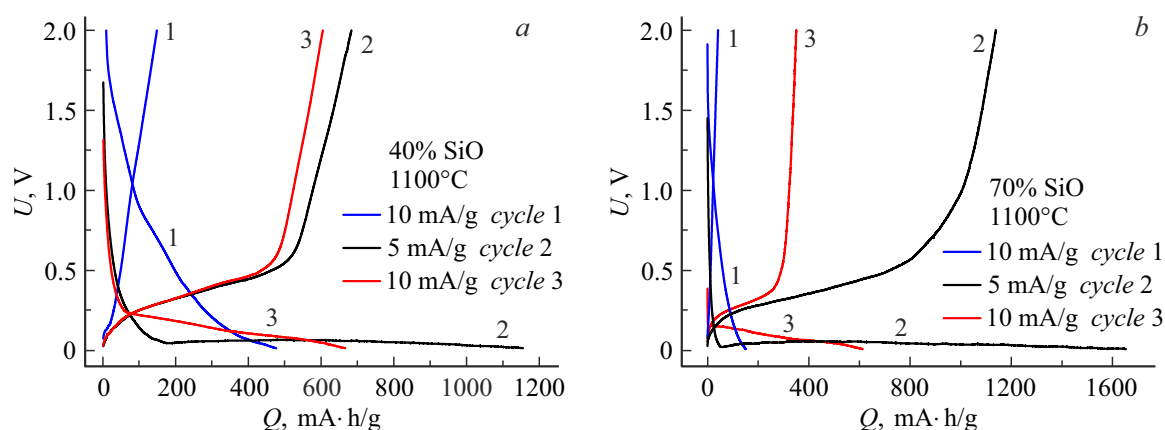
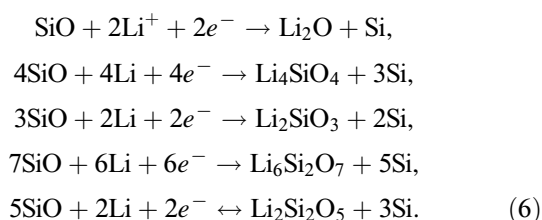


**Figure 8.** Charge/discharge curves for samples, annealed at  $T = 1100^\circ\text{C}$ , for current: 10 (1st cycle), 5 (2nd cycle) and 10 mA/g (3rd cycle): *a* — sample with initial composition of 40% SiO, *b* — 70% SiO.

values side, while  $x$  increases. In the majority of works such a shift of charge/discharge curves is explained with high overpotential of reaction of lithium implementation to SiO electrodes. The reason behind this overpotential, according to authors of [9,29], is a low electronic conductivity of SiO<sub>2</sub>, formed at disproportionation of SiO, while authors of [26] think that it is caused by Si appearing.

Carbonization temperature increase results in growth of Coulomb efficiency of electrodes at the first cycle (Fig. 11). It is well known, that electrodes based on silicon monoxide have low CE value, since at the first lithium implementation the formation of irreversible phases of Li<sub>2</sub>O and lithium silicates is performed with release of nano-scale silicon, that is capable to reversible lithiation [4]:



It should be noted, that not all consider the last reaction as reversible [9]. Disproportionation results in decrease of the weight content of SiO phase, participating in irreversible lithium implementation, and as a result, CE increase is observed.

Operability at higher currents for anodes, annealed at various temperature, can be evaluated as per data, presented in Fig. 12. It is shown, that for samples after disproportionation the decrease of  $Q_{\text{dch}}$  at current density increase is less, than for samples, carbonized at 800°C. In other words, annealing temperature increase results in improving of the rate capability of the electrodes (except for the 1st cycle).

## 5. Analysis of irreversible losses of the 1st cycle

Let's separate the contribution of various components to the irreversible capacity value. For that from the data of galvanostatic measurements we calculate the overall irreversible capacity of the first cycle, spent on SEI

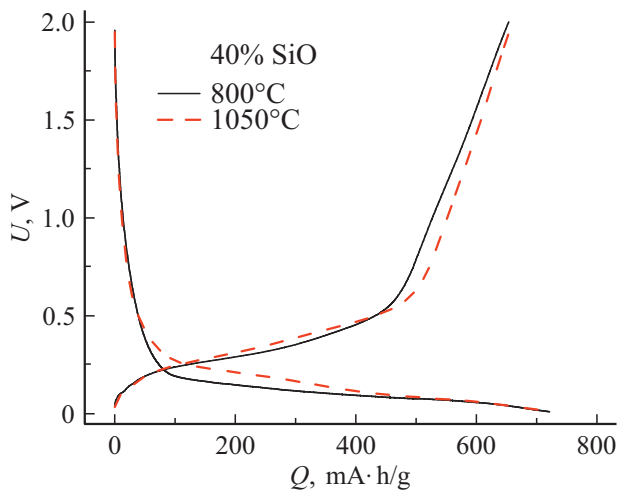


**Figure 9.** Charge/discharge curves of the 2nd cycle for samples with initial composition of 40% SiO, annealed at two different temperatures,  $j = 10$  mA/g.

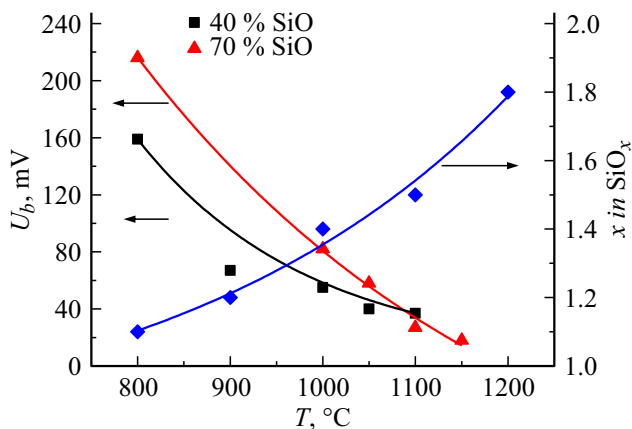
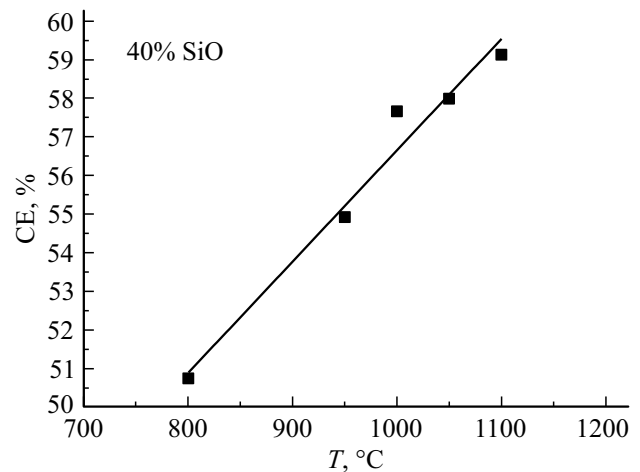


**Figure 10.** Dependence of voltage  $U_b$  on annealing temperature at first lithiation. The right axis shows how  $\text{SiO}_x$  matrix composition changes with temperature.

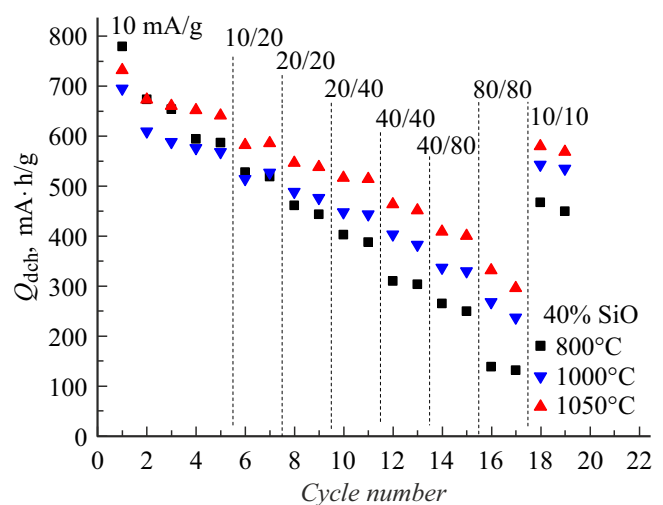
creation and formation of silicates and single lithium oxide,  $Q_{\text{irr}} = Q_{\text{ch}} - Q_{\text{dch}}$ . Dividing  $Q_{\text{irr}}$  by the percentage content of SiO in the end product  $s$ , we obtain the specific irreversible losses  $Q_s$  per weight unit of SiO. Figure 13 shows the obtained dependencies in semi-logarithmic scale.

By means of extrapolation of plots, presented in Fig. 13, to  $s = 100\%$  we find the capacity  $Q_{s100}$ , that characterizes the specific losses per weight unit of SiO in carbon-free material (intrinsic losses, appearing as a result of conversion reaction with formation of irreversible lithium compounds). For samples, annealed at  $800^\circ\text{C}$ , internal specific losses are  $Q_{s100} = 474$  mA·h/g, while for annealed at  $1050^\circ\text{C}$  they are less  $Q_{s100} = 339$  mA·h/g. Assuming, that these values represent only internal losses, since SEI losses for pure SiO due to its extremely small surface area can be neglected, we find the total internal losses for samples with various content of silicon monoxide

by multiplying  $Q_{s100}$  by SiO content in the finished product of carbonization reaction  $Q_{\text{int}} = s \cdot Q_{s100}$ . Therefore, the losses due to SEI are the difference between overall and internal losses  $Q_{\text{SEI}} = Q_{\text{irr}} - Q_{\text{int}}$ . Figure 14 shows that annealing temperature increase results in significant reduction of SEI losses, which are manifested stronger for compositions with less SiO content. Difference of SEI losses between SiO/C and  $d$ -SiO/C can not be explained by surface area reduction only. For instance, for samples with 40% SiO in initial powder ( $s = 49.3\%$  SiO in reaction product) the SEI losses at annealing temperature increase were reduced by 30%, while the surface area was reduced  $\sim$  by 12% only. Therefore, the annealing temperature increase mainly influences the carbon component of the composite, prop-



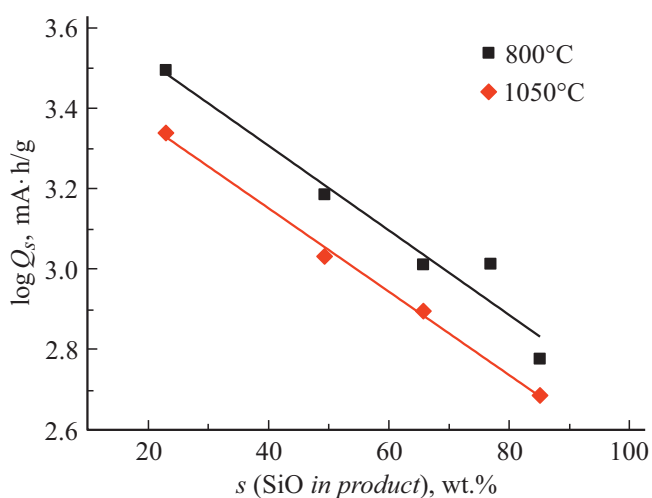
**Figure 11.** Dependence of Coulomb efficiency of the first cycle from annealing temperature for samples with initial concentration of 40% SiO. Density of charge/discharge current is 10 mA/g for  $T < 1100^\circ\text{C}$ , 5 mA/g — for  $T \geq 1100^\circ\text{C}$ .



**Figure 12.** Dependence of discharge capacity on cycle number at various current density for electrodes made of initial mixture with 40% SiO and heat treated at various temperature.

**Table 3.** Irreversible losses of the 1st cycle depending on SiO content for composites, annealed at two different temperatures

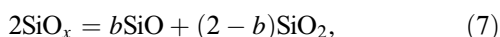
% SiO		800°C				1050°C			
$s_i$ in initial composition	$s$ in product	$Q_{irr}$ , mA·h/g	$Q_s$ , mA·h/g	$Q_{int}$ , mA·h/g	$Q_{SEI}$ , mA·h/g	$Q_{irr}$ , mA·h/g	$Q_s$ , mA·h/g	$Q_{int}$ , mA·h/g	$Q_{SEI}$ , mA·h/g
30	22.9	719	3125	109	607	499	2180	78	422
40	49.3	757	1535	234	523	530	1076	167	363
50	65.7	675	1028	312	364	518	787	223	294
60	76.9	793	1031	365	428			260	–
70	85.1	510	599	404	106	413	486	288	125
100	100	474	474	474	–	339	339	339	–

**Figure 13.** Dependence of specific irreversible capacity  $Q_s$  on calculated SiO content in composite.

erties of which are changed so, that SEI losses decrease. During analysis of spectra of Raman scattering in SiO/C material [22] only small increase of carbon shell graphitization degree with temperature was revealed, that hardly could significantly influence the SEI formation process.

The observed data on irreversible losses of the first cycle are summarized in Table 3. They indicate the less intrinsic losses due to formation of lithium oxide and its silicates in samples, annealed at higher temperature. The reason is the disproportionation of SiO. At electrode charge only silicon monoxide irreversibly reacts with lithium, while silicon dioxide is inert, and reaction with nano-silicon is reversible [27]. If internal irreversible losses are related with SiO monoxide only, they should be proportional to its weight percentage.

SiO<sub>x</sub> matrix can be presented as a two-component system, consisting of undercomposed monoxide part with molar fraction  $b$  and silicon dioxide

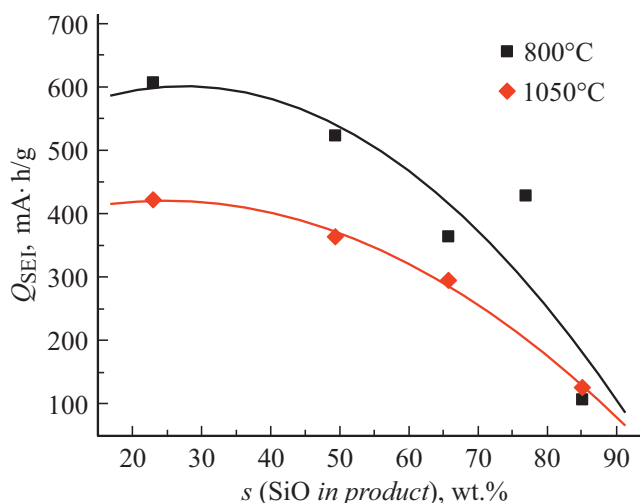


from which it follows that  $b = 2(2 - x)$ , and weight fraction of undercomposed SiO is

$$k = (2 - x)M_{\text{SiO}} / (A_{\text{Si}} + xA_{\text{O}}), \quad (8)$$

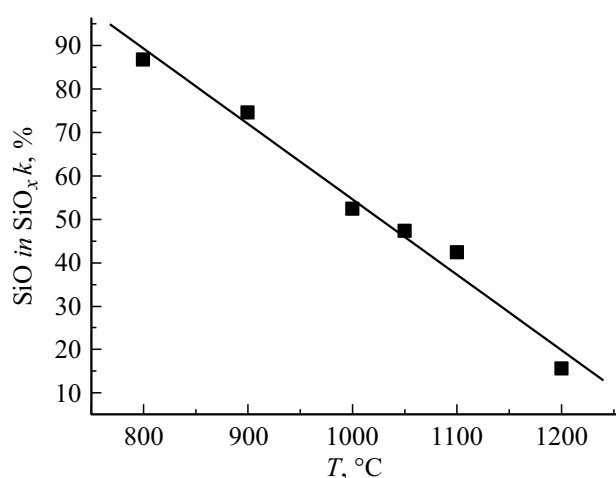
where  $M_{\text{SiO}}$  is molecular mass of SiO,  $A_{\text{Si}}$  and  $A_{\text{O}}$  are atomic masses of silicon and oxygen respectively. Using data from our work [23] on temperature dependence of SiO<sub>x</sub> matrix composition, we obtain the percentage content of SiO depending on annealing temperature, which are presented in Table 4 and in Fig. 15.

Figure 16 shows values of irreversible losses, caused by conversion reactions and electrolyte reduction, as well as total irreversible losses depending on composite content. In Figs. 16, c and 16, d the stars indicate the values of internal surface of composites (values from Table 1), which are in good agreement with curves for  $Q_{\text{SEI}}$ . Thus, it confirms, that irreversible losses due to SEI formation are related to heavily increasing surface area in samples with high carbon content.

**Figure 14.** Dependence of irreversible capacity part, caused by SEI, on SiO content in the composite.

**Table 4.** Dependence of amount of released silicon, its precipitates size, number of oxygen moles  $x$  in matrix of  $\text{SiO}_x$  [23] and weight fraction  $k$  of undercomposed SiO on annealing temperature

$T, ^\circ\text{C}$	Quantity of Si, w%	Diameter of Si precipitates, nm	$x$ in $\text{SiO}_x$ matrix	$k$ (SiO in $\text{SiO}_x$ ), w%
ini	6.7	3.6	1.0	100
800	10.3	3.3	1.1	86.8
900	19.0	3.5	1.2	74.6
1000	25.0	4.3	1.4	52.4
1050	27.5	5.9	1.45	47.3
1100	28.3	7.8	1.5	42.3
1200	34.6	13.4	1.8	15.5

**Figure 15.** Part of undercomposed silicon monoxide  $k$  depending on annealing temperature.

## 6. Electrochemical impedance spectroscopy

For studying the influence of annealing temperature on lithium implementation process in SiO/C and  $d$ -SiO/C the impedance measurements were performed on electrodes with initial content of 40 wt% SiO, annealed at two temperatures. After completion of Li implementation process, i.e. upon reaching the restrictive voltage of 10 mV, the electrode was disconnected from the stand and relaxed in current-free mode within several hours. As a result of relaxation the voltage  $U = 90$  mV was set on it. After that the impedance measurements were performed. Charge of 1100-degr. sample at the first cycle was performed with current density of 5 mA/g, 800-degr. — with 10 mA/g, at the following cycles for both samples  $j = 10$  mA/g. The observed hodographs in Nyquist coordinates are presented in Fig. 17. The diagrams show that disproportionation results in decrease of electrodes impedance.

Low-frequency part of hodographs is a line with a slope, close to  $\sim 45^\circ$ . In this case from the measured values of imaginary component of impedance ( $\text{Im}Z$ ), it is possible

to define the value of Warburg constant (9) and make calculation of effective diffusion coefficient for atoms of lithium  $D$  [30,31]:

$$W = -\text{Im}Z\sqrt{2\pi f}, \quad (9)$$

where  $W$  is Warburg constant, [ $\text{Ohm}\cdot\text{s}^{-0.5}\cdot\text{cm}^2$ ];  $f$  is alternating voltage frequency, [ $\text{s}^{-1}$ ].

Warburg constant, in its turn, depends on equilibrium potential  $E$  and concentration of diffusing Li [mol/l] as per equation

$$W = (|dE/dc|)/nF\sqrt{2D}, \quad (10)$$

where  $E$ ,  $n$ ,  $F$  and  $D$  are potential, number of electrons, participating in electrochemical reaction, Faraday constant and lithium diffusion coefficient respectively. Connection between  $E$  and  $c$  is defined from quasi-equilibrium charge curve, i.e. dependence of  $E$  on implemented charge  $Q$ . In our case  $E$  can be replaced with  $U$  due to insignificant polarization of lithium electrode. In rather wide range of capacity the dependence of  $U$  on  $Q$  is close to linear (Figs. 7,  $a$  and 8,  $a$ ):

$$dQ = (dc nF)/\rho, \quad (11)$$

where  $\rho$  is composite density, [ $\text{g}/\text{cm}^3$ ].

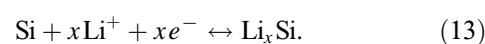
Slope of the flat section of the galvanostatic charge curve  $dU/dQ$  and replacement of  $dc$  with  $dQ$  from relation (10) give the following equation for calculation of diffusion coefficient:

$$D = (dU/dQ)^2/(2\rho^2 \cdot W^2). \quad (12)$$

Diffusion coefficient calculation results are presented in Table 5. The observed values of the diffusion coefficient  $D$  correspond to data of other authors for anode materials based on SiO, used the same method of determination of  $D$  [32], but significantly lower, than in materials based on silicon [33]. Effective diffusion coefficient for Li in  $d$ -SiO/C at the 1st cycle is lower, than in SiO/C, that during the charge process results in increase of lithium concentration in near-surface part of the electrode and as per Nernst equation — to reduction of voltage  $U$ , the latter explains shifting of charge curves with increase of  $T$  (Fig. 7,  $a$ ). According to data from Table 5, at the 3rd cycle  $D$  for electrodes of  $d$ -SiO/C heavily increases and remains the same value at the following cycles, while for samples of SiO/C the diffusion coefficient is almost the same.

## 7. Discussion of results

As known [4], the mechanism of the first electrochemical lithiation of SiO is divided into two successive steps: 1) conversion reaction (6) between silicon monoxide and lithium ions with formation of  $\text{Li}_2\text{O}$ , lithium silicates and nano-silicon; 2) reaction of formation of intermetallic compounds of  $\text{Li}_x\text{Si}$  between lithium and nano-silicon



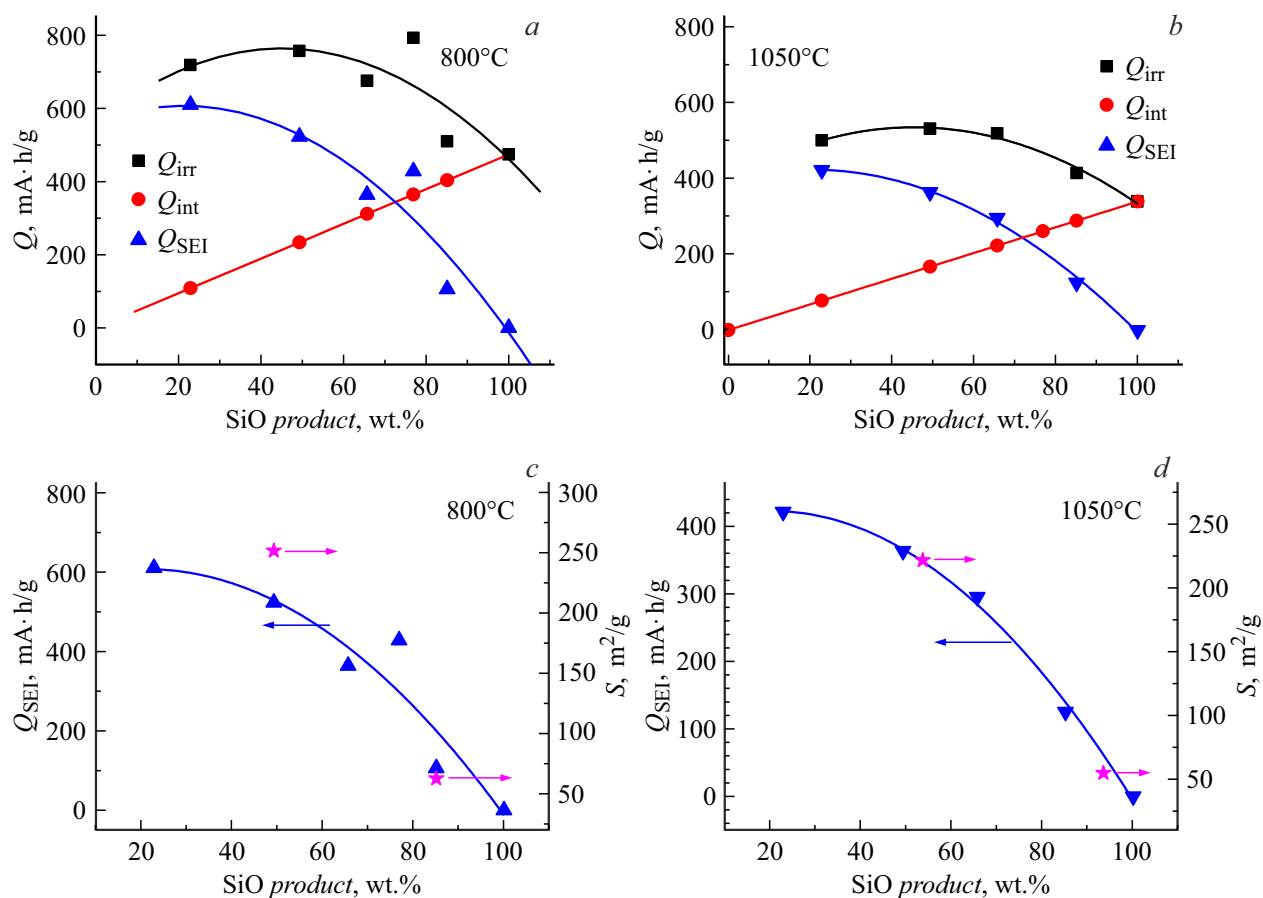


**Figure 16.** Dependence of irreversible losses of the first cycle on composition of the finished composite:  $Q_{irr}$  — total losses,  $Q_{int}$  — intrinsic losses,  $Q_{SEI}$  — losses due to formation of SEI: *a* and *b* — for samples, annealed respectively at 800 and 1050°C; *c* and *d* — comparison of SEI losses with specific surface area for material of two compositions (indicated with stars and right axis).

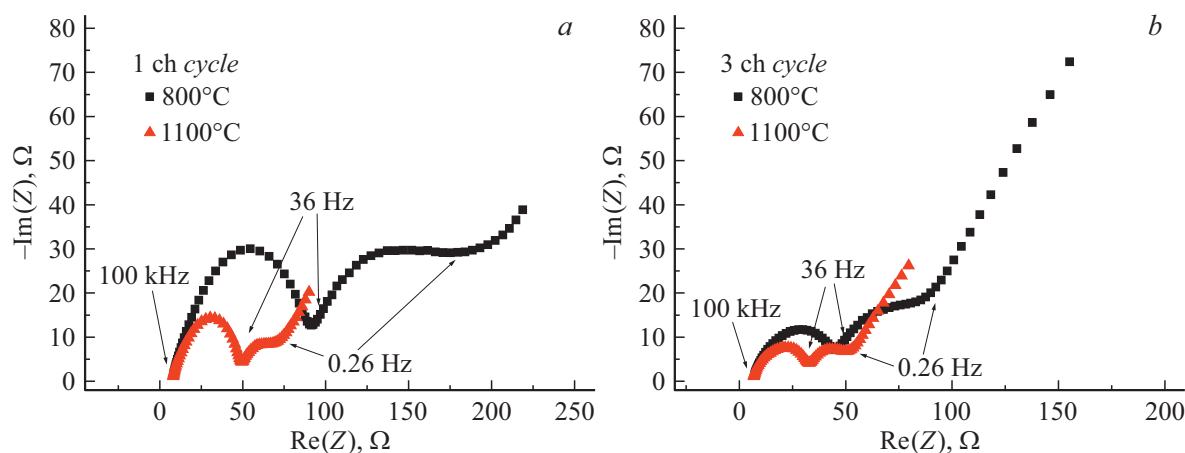


**Figure 17.** Impedance hodographs for samples of SiO/C and *d*-SiO/C: *a* — at the 1st cycle, *b* — at the 3rd cycle.

According to work [9], at the first charge the silicates and lithium oxide are formed at voltage of 1.0–1.4 V, while compounds of  $\text{Li}_x\text{Si}$  — at  $U = 0.22\text{--}0.37$  V. The first process is irreversible, while the second — reversible. Lithium implementation into carbon component of the composite also happens at low potential of  $< 0.24$  V [34,35],

but its contribution to capacity is small compared to Si. Actually, in cycles after the first one the same process of implementation and extraction of Li prevails (14), as in the case of silicon electrodes. This process explains the difference in shape of charge curves for the 1st, 2nd and 3rd cycles in high-temperature *d*-SiO/C anodes

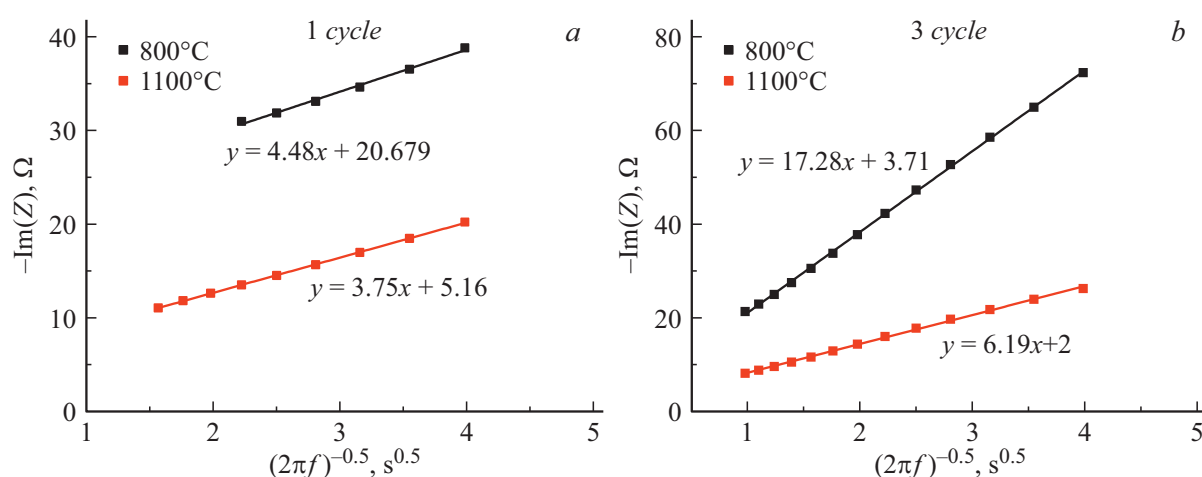


**Figure 18.** Dependence of  $-\text{Im}Z$  on  $1/\sqrt{2\pi f}$  for low-frequency part of impedance hodographs of Fig. 17: *a* — 1st cycle, *b* — 3rd cycle.

**Table 5.** Parameters, observed by processing of EIS spectra and galvanostatic charge curves for samples with initial composition of 40% SiO

Nº of cycle	Composite	$T, ^\circ\text{C}$	$W, \Omega \cdot \text{s}^{-0.5} \cdot \text{cm}^2$	$dU/dQ, \Omega \cdot \text{g/s}$	$D, \text{cm}^2/\text{s}$
1	SiO/C	800	$3.2 \cdot 10^4$	$2 \cdot 10^{-3}$	$2.7 \cdot 10^{-15}$
	<i>d</i> -SiO/C	1100	$3 \cdot 10^4$	$2.6 \cdot 10^{-4}$	$4.8 \cdot 10^{-17}$
3	SiO/C	800	$1.2 \cdot 10^5$	$4.5 \cdot 10^{-3}$	$8.4 \cdot 10^{-16}$
	<i>d</i> -SiO/C	1100	$4.9 \cdot 10^4$	$7.5 \cdot 10^{-3}$	$5.1 \cdot 10^{-14}$

**Table 6.** Structure of lithiated silicon particles in composites, formed at  $T = 800$  and  $1100^\circ\text{C}$ , at the 1st and the following cycles

Composite	$T, ^\circ\text{C}$	1st cycle	3rd cycle
SiO/C	800		
<i>d</i> -SiO/C	1100		

(Fig. 8). There is no plateau entering at the first cycle and, since the discharge capacity is extremely low, the conclusion can be made, that the reversible reaction of  $\text{Li}_x\text{Si}$  formation does not happen. At lower current at the second cycle the horizontal plateau appears, corresponding to the reversible lithiation of silicon. Horizontal section at the charge curve is specific for anode materials, in which

lithiation is performed in two-phase system [1]. Lack of slope in this section of  $U = f(Q_{\text{ch}})$  curve, according to model [36], indicates that the limiting factor of the process is a boundary progression rate between lithiated amorphous layer and remaining volume of crystalline silicon (Table 6). Such behavior is caused by significantly higher mobility of lithium in amorphous phase with high lithium content,

than in crystalline silicon [37]. Crystallinity of silicon precipitates, formed at disproportionation, is confirmed with data of XRD analysis [23]. According to Table 4, their size increases with annealing temperature increase. Thus, the first lithiation of large Si precipitates in *d*-SiO/C happens by two-phase mechanism, while during lithiation of SiO/C with small Si particles two phases do not appear, and the corresponding section of the charge curve significantly shifts from horizontal. Indeed, in SiO/C samples the slope of the flat section of the charge curve exists at the first lithiation already (Fig. 3, *a*), indicating the initially amorphous condition of Si nano-particles, formed as a result of SiO reaction with Li.

At the 3rd and the following cycles in *d*-SiO/C composites this section obtains significant slope (Figs. 8, 9, as well as values of  $dU/dQ$  in Table 5), that can be explained with thorough amorphization of silicon particles and disappearance of the above mentioned boundary. At *d*-SiO/C anodes forming the long flat section on the charge curve appears at low voltage. The latter indicates that the main reason of lithium diffusion coefficient increase and improvement of rate capability of *d*-SiO/C anodes after forming is amorphization of silicon clusters, not formation of  $\text{Li}_4\text{SiO}_4$  silicate, that, according to some authors, has high conductivity of Li ions [9,38]. The capability of the finished composites to operate at increased current is still rather low, that does not agree with literature data on higher, compared to silicon, rate of charge/discharge and prospectivity of anodes based on SiO for powerful cells [38].

Difference between the mechanisms of the first lithiation of SiO/C and *d*-SiO/C is also reflected on the observed values of diffusion coefficient. In case of two-phase mechanism of the first lithiation in 1100-degr. sample the low  $D$  is actually some effective value, defined by reaction rate at the boundary of amorphous-crystalline Si, that, in its turn, depends on the charge current. It is not surprising, that in *d*-SiO/C at the following cycles, with the change of lithiation mechanism,  $D$  increases by an order of 3. At the same time, it is unclear, why for SiO/C sample the low value of  $D$  remains at the 3rd cycle. The above mentioned allows to make a conclusion, that diffusion conditions in silicon particles, containing in *d*-SiO/C and SiO/C, are different. In case of *d*-SiO/C the concentration of lithium in Si particles should be higher, since  $\text{SiO}_2$ , containing in composite, is inert, and with the same specific capacity the more lithium accounts for the active part of anode mass. And higher level of lithiation usually contributes to higher mobility of Li.

## Conclusions

According to study of anode parameters depending on composition, the composites with initial content of SiO 30–50% show best results.

Annealing at  $T = 1000\text{--}1100^\circ\text{C}$ , when the partial disproportionation of silicon monoxide happens, results in increase of the first cycle efficiency, increase of discharge capacity

at the following cycles and capability to operate at higher current compared to SiO/C composites, made at  $T = 800^\circ\text{C}$ .

Annealing temperature increase is accompanied with Si precipitates size increase, increase of part of  $\text{SiO}_2$ , inert to Li, and decrease of SiO content, participating in irreversible conversion reactions. All these changes define potential, at which Li implementation is performed, decrease part of intrinsic irreversible losses at the first cycle, and result in increase of lithium diffusion coefficient in *d*-SiO/C composites at the following cycles.

Observed in the work [22] sharp drop of charge capacity  $Q_{\text{ch}}$  for *d*-SiO/C composites, annealed at  $T > 1100^\circ\text{C}$ , is explained not with abrupt change of anode material properties, but is a result of combination of smoothly reducing voltage of plateau reaching at the first lithiation and the selected measurement conditions (restrictions of 10 mV at charge).

Irreversible losses of the 1st cycle of the studied samples consist of intrinsic losses, caused by SiO conversion reaction during interaction with Li, and SEI formation losses. Analysis showed that the first ones increase with SiO concentration increase, while the seconds ones, on the contrary, decrease due to reduction of portion of carbon with large surface area.

It was revealed that the forming of high-temperature *d*-SiO/C anodes at the 1st cycle with low charge current results in  $Q_{\text{ch}}$  increase to values, specific for samples, annealed at lower temperatures. Large change of kinetic parameters of *d*-SiO/C anodes after completion of forming is explained with amorphization of silicon crystallites and increase of lithium diffusion coefficient  $D$ .

## Acknowledgments

Authors would like to thank M.V. Tomkovich and Yu.A. Kukushkina for the performed BET studies and M.P. Karusheva for help with EIS measurements studies.

## Conflict of interest

The authors declare that they have no conflict of interest.

## References

- [1] M.N. Obrovac, V.L. Chevrier. Chem. Rev., **114**, 11444 (2014). DOI: 10.1021/cr500207g
- [2] Zh. Liu, Q. Yu, Y. Zhao, R. He, M. Xu, S. Feng, S. Li, L. Zhou, L. Mai. Chem. Soc. Rev., **48**, 285 (2019). DOI: 10.1039/c8cs00441b
- [3] T. Chen, J. Wu, Q. Zhang, X. Su. J. Power Sources, **363**, 126 (2017). DOI: 10.1016/j.jpowsour.2017.07.073
- [4] M. Jiao, Y. Wang, C. Ye, C. Wang, W. Zhang, C. Liang. J. Alloy. Compd., **842**, 155774 (2020). DOI: 10.1016/j.jallcom.2020.155774
- [5] J.-H. Kim, C.-M. Park, H. Kim, Y.-J. Kim, H.-J. Sohn. J. Electroanal. Chem., **661**, 245 (2011). DOI: 10.1016/j.jelechem.2011.08.010

- [6] S.C. Jung, H.-J. Kim, J.-H. Kim, Y.-K. Han. *J. Phys. Chem. C.*, **120** (2), 886 (2016). DOI: 10.1021/acs.jpcc.5b10589
- [7] Y. Nagao, H. Sakaguchi, H. Honda, T. Fukunaga, T. Esaka. *J. Electrochem. Soc.*, **151** (10), A1572 (2004). DOI: 10.1149/1.1787173
- [8] M. Miyachi, H. Yamamoto, H. Kawai, T. Ohta, M. Shirakata. *J. Electrochem. Soc.*, **152** (10), A2089 (2005). DOI: 10.1149/1.2013210
- [9] K. Yasuda, Y. Kashitani, S. Kizaki, K. Takeshita, T. Fujita, S. Shimosaki. *J. Power Sources*, **329**, 462 (2016). DOI: 10.1016/j.jpowsour.2016.08.110
- [10] L.Y. Beaulieu, K.W. Eberman, R.L. Turner, L.J. Krause, J.R. Dahna. *Electrochem. Solid-State Lett.*, **4** (9), A137 (2001). DOI: 10.1149/1.1388178
- [11] T. Kim, S. Park, S.M. Oh. *J. Electrochem. Soc.*, **154**, A1112 (2007). DOI: 10.1149/1.2790282
- [12] Y. Yamada, Y. Iriyama, T. Abe, Z. Ogumi. *J. Electrochem. Soc.*, **157** (1), A26 (2010). DOI: 10.1149/1.3247598
- [13] J. Cui, Y. Cui, S. Li, H. Sun, Z. Wen, J. Sun. *ACS Appl. Mater. Interfaces*, **8** (44), 30239 (2016). DOI: 10.1021/acsami.6b10260
- [14] Q. Yuan, F. Zhao, Y. Zhao, Z. Liang, D. Yan. *Electrochimica Acta*, **115**, 16 (2014). DOI: 10.1016/j.electacta.2013.10.106
- [15] M. Yamada, A. Ueda, K. Matsumoto, T. Ohzuku. *J. Electrochem. Soc.*, **158** (4), A417 (2011). DOI: 10.1149/1.3551539
- [16] T. Xu, Q. Wang, J. Zhang, X. Xie, B. Xia. *ACS Appl. Mater. Interfac.*, **11**, 19959 (2019). DOI: 10.1021/acsami.9b03070
- [17] L. Guo, H. He, Y. Ren, C. Wang, M. Li. *Chem Eng. J.*, **335**, 32 (2017). DOI: 10.1016/j.cej.2017.10.145
- [18] L. Hu, W. Xia, R. Tang, R. Hu, L. Ouyang, T. Sun. *H. Wang. Frontiers in Chem.*, **8**, 388 (2020). DOI: 10.3389/fchem.2020.00388
- [19] E.V. Astrova, V.P. Ulin, A.V. Parfeneva, V.B. Voronkov. *Tech. Phys. Lett.*, **45**, 664 (2019). DOI: 10.1134/S1063785019070022
- [20] E.V. Astrova, V.P. Ulin, A.V. Parfeneva, A.M. Rumyantsev, V.B. Voronkov, A.V. Nashchekin, V.N. Nevedomskiy, Y.M. Koshtyal, M.V. Tomkovich. *J. Alloy. Compd.*, **826**, 154242 (2020). DOI: 10.1016/j.jallcom.2020.154242
- [21] E.V. Astrova, V.P. Ulin, A.V. Parfeneva, A.V. Nashchekin, V.N. Nevedomskiy, M.V. Baydakova. *Semiconductors*, **54** (8), 900 (2020). DOI: 10.1134/S1063782620080059
- [22] D.A. Lozhkina, E.V. Astrova, A.I. Likhachev, A.V. Parfeneva, A.M. Ryumyantsev, A.N. Smirnov, V.P. Ulin. *Tech. Phys.*, **91** (9), 1381 (2021). DOI: 10.21883/JTF.2021.09.51218.83-21
- [23] D.A. Lozhkina, E.V. Astrova, R.V. Sokolov, D.A. Kirilenko, A.A. Levin, A.V. Parfeneva, V.P. Ulin. *Semiconductors*, **55** (4), 373 (2021). DOI: 10.1134/S1063782621040096
- [24] A.S. Fialkov. *Uglerod, mezhsloevye soedineniya i kompozity na ego osnove* (Aspekt Press, M., 1997), p. 377–404 (in Russian).
- [25] M. Winter, P. Novák, A. Monnier. *J. Electrochem. Soc.*, **145**, 428 (1998). DOI: 10.1149/1.1838281
- [26] T. Tan, P.-K. Lee, D.Y.W. Yu. *J. Electrochem. Soc.*, **166**—(3), A5210 (2019). DOI: 10.1149/2.0321903jes
- [27] J. Yang, Y. Takeda, N. Imanishi, C. Capiglia, J.Y. Xie, O. Yamamoto. *Solid State Ionics*, **152–153**, 125 (2002). DOI: 10.1016/S0167-2738(02)00362-4
- [28] Ch.-M. Park, W. Choi, Y. Hwa, J.-H. Kim, G. Jeong, H.-J. Sohn. *J. Mater. Chem.*, **20**, 4854 (2010). DOI: 10.1039/B923926J
- [29] K. Kitada, O. Pecher, P.C.M.M. Magusin, M.F. Groh, R.S. Weatherup, C.P. Grey. *J. Am. Chem. Soc.*, **141**, 7014 (2019). DOI: 10.1021/jacs.9b01589
- [30] Z.B. Stojnov, B.M. Grafov, B.S. Savova-Stojnova, V.V. Elkin. *Elektrokhimicheskij impedans* (Nauka, M., 1991), p. 336 (in Russian).
- [31] A.V. Churikov, K.I. Pridatko, A.V. Ivanishchev, I.A. Ivanishcheva, I.M. Gamayunova, K.V. Zapsis, V.O. Sycheva. *Elektrokhimiya*, **44** (5), 594 (2008) (in Russian). DOI: 10.1134/S1023193508050078
- [32] M. Xia, L. Yi-ran, X. Xiong, W. Hu, Y. Tang, N. Zhou, Z. Zhou, H. Zhang. *J. Alloy. Compd.*, **800**, 116e124 (2019). DOI: 10.1016/j.jallcom.2019.05.365
- [33] F. Ozanam, M. Rosso. *Mat. Sci. Eng.*, **213**, 2 (2016). DOI: 10.1016/j.mseb.2016.04.016
- [34] H. Yang, F. Fan, W. Liang, X. Guo, T. Zhu, S. Zhang. *J. Mech. Phys. Sol.*, **70**, 349 (2014). DOI: 10.1016/j.jmps.2014.06.004
- [35] S. Yoshida, T. Okubo, Y. Masuo, Y. Oba, D. Shibata, M. Haruta, T. Doi, M. Inaba. *Electrochemistry*, **85** (7), 403 (2017). DOI: 10.5796/electrochemistry.85.403
- [36] M. Pharr, K. Zhao, X. Wang, Z. Suo, J.J. Vlassak. *Nano Lett.*, **12** (9), 5039 (2012). DOI: 10.1021/nl302841y
- [37] J. Park, S.S. Park, Y.S. Won. *Electrochim. Acta*, **107**, 467 (2013). DOI: <https://doi.org/10.1016/j.electacta.2013.06.059>
- [38] K. Pan, F. Zou, M. Canova, Y. Zhu, J.-H. Kim. *J. Power Sources*, **413**, 20 (2019). DOI: 10.1016/j.jpowsour.2018.12.010